Torsten Aigner, BSc.

Influence of a singular joint with variable length and distance in relation to the excavation diameter on the displacements of tunnels

Master's Thesis

Submitted in fulfilment of the requirements for the degree of

Diplom-Ingenieur

Master's programme Civil Engineering, Geotechnical and Hydraulic Engineering

at

Graz University of Technology

Supervisor

O.Univ.-Prof. Dipl.-Ing. Dr.mont. Wulf Schubert

Institute of Rock Mechanics and Tunnelling

Graz University of Technology

Graz, October 2018

EIDESSTATTLICHE ERKLÄRUNG
AFFIDAVIT

Ich erkläre an Eides statt, dass ich die vorliegende Arbeit selbstständig verfasst, andere als die angegebenen Quellen/Hilfsmittel nicht benutzt, und die den benutzten Quellen wörtlich und inhaltlich entnommenen Stellen als solche kenntlich gemacht habe. Das in TUGRAZonline hochgeladene Textdokument ist mit der vorliegenden Masterarbeit identisch.

I declare that I have authored this thesis independently, that I have not used other than the declared sources/resources, and that I have explicitly indicated all material which has been quoted either literally or by content from the sources used. The text document uploaded to TUGRAZonline is identical to the present master‘s thesis.

Datum / Date	Unterschrift / Signature

Acknowledgements

First of all, I would like to thank all people, who encouraged and accompanied me from the beginning of my studies to the diploma. My biggest thanks go to my girlfriend Christiane, who has always supported me mentally and especially financially in difficult life situations. Without her help I would not have been able to finish my studies.

Furthermore, I would like to thank my parents Renate and Norbert, especially my mother Renate, who I want to thank from the bottom of my heart. Without her help and support during the summers this would never have been possible.

A special thanks applies to my deceased grandfather Friedrich, who always had an open ear for my feelings, thoughts and problems.

Furthermore, a great help during my studies were my best friends Julian and Alexander as well as Bernhard for the amazing time we could spent together.

Finally, I want to thank my supervisor Wulf Schubert, who has raised my interest in tunnelling and rock mechanics in a unique way and has always been helpful in different situations.

Therefore, thank you and “Glück auf!”

Abstract

This master thesis deals with the investigation of the range of influence of a singular joint, which is approached by a tunnel excavation. Aim is identifying combinations of length and distance from the tunnel perimeter of single discontinuities with low shear strength, having a significant influence on the tunnel deformations. An isotropic plastic material behaviour with Mohr-Coulomb failure criterion for the rock mass was used for the numerical simulation in the software Phase^2 (Rocscience, 2014). The different joint distances and length were simulated with joint elements with a Mohr-Coulomb slip criterion for the activated and a material dependent slip criterion for the deactivated joint elements. The investigation was done with the same mesh for all calculations. For allowing a general use for different tunnel diameters, the distance and the length of the joint were related to the excavation diameter. Additionally, the influence of different K_0 values and Young's Moduli are investigated in this thesis.

Kurzfassung

Die vorliegende Masterarbeit führt eine Untersuchung über den Einflussbereich einer singulären Trennfläche mit geringer Scherfestigkeit durch, welcher sich ein Tunnelausbruch annähert. Es sollte festgestellt werden, welche Kombinationen von Trennflächenlänge und Abstand der Trennfläche zum Ausbruchsrand einen signifikanten Einfluss auf die Verschiebungen des Tunnels hat. Die Auswertung erfolgt hauptsächlich durch die maximalen Verschiebungen, die durch unterschiedliche Konstellationen des Abstandes sowie der Länge der Trennfläche verursacht werden. Für die numerische Simulation mit der Software Phase^2 (Rocscience, 2014) wurde ein Material mit isotropem, plastischen Materialverhalten und dem Mohr Coulomb Bruchkriterium verwendet. Die verschiedenen Abstände und Längen der Trennfläche wurden mittels Joint Elements simuliert. Das Mohr-Coulomb Gleitkriterium wurde für die aktivierten Trennflächensegmente und ein materialabhängiges Gleitkriterium für die deaktivierten Trennflächensegmente angewendet. Für die Untersuchung wurde für alle Berechnungen das gleiche Netz verwendet. Um einen allgemeinen Vergleich mit anderen Tunneldurchmessern zu ermöglichen, wurde der Trennflächenabstand zum Ausbruchsrand, sowie die Trennflächenlänge auf den Ausbruchdurchmesser normiert. Des Weiteres wurde beurteilt, ob eine singuläre Trennfläche einen signifikanten Einfluss auf die Verschiebungen hat. Zusätzlich wurde noch der Einfluss der Änderung des Seitendruckwerts und des Elastizitätsmoduls untersucht.

Table of Contents

List of figures

List of tables

Symbols

c ..... Cohesion [MPa]

c_{joint} ..... Cohesion of the joint segment [MPa]

$c_{joint,act}$ ..... Cohesion of the activated joint segment [MPa]

$c_{joint,act,peak}$ ..... Peak cohesion of the activated joint segment [MPa]

$c_{joint,act,res}$ ..... Residual cohesion of the activated joint segment [MPa]

$c_{joint,deact}$ ..... Cohesion of the deactivated joint segment [MPa]

$c_{joint,deact,peak}$ ... Peak cohesion of the deactivated joint segment [MPa]

$c_{joint,deact,res}$ ..... Residual cohesion of the deactivated joint segment [MPa]

c_{rock} ..... Cohesion of the rock material [MPa]

$c_{rock,peak}$ ..... Peak cohesion of the rock material [MPa]

$c_{rock,res}$ ..... Residual cohesion of the rock material [MPa]

Ci ..... Interface coefficient [-]

Cs ..... Stiffness coefficient [-]

D..... Tunnel diameter [m]

E ..... Young`s Modulus [MPa]

E_{rock} ..... Young`s Modulus of the rock material [MPa]

$E_{rock1,peak}$ ..... Peak Young`s Modulus of the rock material 1 [MPa]

$E_{rock1,res}$ ..... Residual Young`s Modulus of the rock material 1 [MPa]

$E_{rock2,peak}$ ..... Peak Young`s Modulus of the rock material 2 [MPa]

$E_{rock2,res}$ ..... Residual Young`s Modulus of the rock material 2 [MPa]

K_0 ..... Coefficient of the lateral pressure [-]

Kn_{act} ..... Joint normal stiffness of activated joint segment [MPa/m]

Kn_{deact} ..... Joint normal stiffness of deactivated joint segment [MPa/m]

$Kn_{deact,peak}$ ..... Peak joint normal stiffness of deactivated joint segment [MPa/m]

$Kn_{deact,res}$ ..... Residual joint normal stiffness of deactivated joint segment [MPa/m]

Ks_{act} ..... Joint shear stiffness of activated joint segment [MPa/m]

Ks_{deact} ..... Joint shear stiffness of deactivated joint segment [MPa/m]

$Ks_{deact,peak}$ ..... Peak joint shear stiffness of deactivated joint segment [MPa/m]

$Ks_{deact,res}$ ..... Residual joint shear stiffness of deactivated joint segment [MPa/m]

L ..... Joint length [m]

R ..... Distance from the singular joint to the excavation boundary [m]

α ..... Angle between the positive x-axis and direction of σ_1 [°]

$\alpha_{K=0.5}$ ..... Angle between the positive x-axis and direction of σ_1 for $K = 0.5$ [°]

$\alpha_{K=1.0}$ ..... Angle between the positive x-axis and direction of σ_1 for $K = 1.0$ [°]

ν ..... Poisson's ratio [-]

ν_{rock} ..... Poisson's ratio of the rock material [-]

σ_T ..... Tensile strength [MPa]

$\sigma_{T,joint}$ ..... Tensile strength of the joint material [MPa]

$\sigma_{T,joint,act}$ ..... Tensile strength of the activated joint material [MPa]

$\sigma_{T,joint,act,peak}$ ... Peak tensile strength of the activated joint material [MPa]

$\sigma_{T,joint,act,res}$ ..... Residual tensile strength of the activated joint material [MPa]

$\sigma_{T,rock}$ ..... Tensile strength of the rock material [MPa]

$\sigma_{T,rock,peak}$ ..... Peak tensile strength of the rock material [MPa]

$\sigma_{T,rock,res}$ ..... Residual tensile strength of the rock material [MPa]

σ_Z ..... Out-of-plane field stress [MPa]

$\sigma_{Z,K=0.5}$ ..... Out-of-plane field stress for $K = 0.5$ [MPa]

$\sigma_{Z,K=1.0}$ ..... Out-of-plane field stress for $K = 1.0$ [MPa]

σ_1 ..... Major in-plane principal field stress [MPa]

$\sigma_{1,K=0.5}$ ..... Major in-plane principal field stress for $K = 0.5$ [MPa]

$\sigma_{1,K=1.0}$ ..... Major in-plane principal field stress for $K = 1.0$ [MPa]

σ_3 ..... Minor in-plane principal field stress [MPa]

$\sigma_{3,K=0.5}$ ..... Minor in-plane principal field stress for $K = 0.5$ [MPa]

$\sigma_{3,K=1.0}$ ..... Minor in-plane principal field stress for $K = 1.0$ [MPa]

φ ..... Friction angle [°]

φ_{joint} ..... Friction angle of the joint segment [°]

$\varphi_{joint,act}$ ..... Friction angle of the activated joint segment [°]

$\varphi_{joint,act,peak}$ ..... Peak friction angle of the activated joint segment [°]

$\varphi_{joint,act,res}$ ..... Residual friction angle of the activated joint segment [°]

$\varphi_{joint,deact}$ ..... Friction angle of the deactivated joint segment [°]

$\varphi_{joint,deact,peak}$ .. Peak friction angle of the activated joint segment [°]

$\varphi_{joint,deact,res}$ .... Residual friction angle of the activated joint segment [°]

φ_{rock} ..... Peak friction angle of the rock material [°]

$\varphi_{rock,peak}$ ..... Peak friction angle of the rock material [°]

$\varphi_{rock,res}$ ..... Residual friction angle of the rock material [°]

ψ ..... Dilation angle [°]

ψ_{rock} ..... Dilation angle of the rock material [°]

1 Introduction

1.1 Aim

The aim of this master thesis is to investigate in which domain a singular joint has a significant influence on the displacements of tunnels. This domain points out when it is reasonable to use a discrete model instead of a smeared model to obtain realistic results. Critical situations in tunnelling in many cases are caused by the excavation approaching a singularity outside the excavation, and hence invisible area. The induced stress increase between excavation boundary and singularity causes larger displacements, and can lead to a failure of the "rock pillar" with the potential of a tunnel collapse. When using a "smeared" rock mass model, the obtained displacements will be homogenous, and critical situations, as described above, will not be detected. For the layout of excavation and support it is essential to know the influence of singularities striking in an acute angle to the tunnel axis.

1.2 Method

The investigation was carried out by numerical simulations in 2D, using the code Phase^2 (Rocscience, 2014). The basis of this investigation are the total displacements, calculated from a basic model, considering a circular tunnel without the influence of a singular joint. Successive models contain singular joints with varying distance and length to the excavation boundary. The properties of the rock mass and joints have been kept constant throughout the investigation, except for the investigation of a lower Young Modulus of the rock mass on the domain of influence.

The results of those models are compared to those of the basic model in various ways.

Results have been normalized to the tunnel diameter for allowing a more general use for different sizes of tunnels.

2 Literature review

2.1 Discontinuity

Discontinuities are a significant part of the rock mass. Overall, “discontinuity” is used as an expression, representative for any delinking of rock blocks with zero or low tensile strength parameters. This designation was first assumed by several authors (Fookes & Parrish, 1969; Attewell & Woodman, 1971; Priest, 1975) without distinguishing their geological origins. The past has shown, that an occurring joint or joint network governs the behaviour of a rock mass more than the rock strength of itself (Palmström, 2001).
Furthermore, Piteau & Jennings, (1970) have listed the discontinuity properties with the greatest influence on the ground behaviour:

- orientation,
- size,
- frequency,
- surface geometry,
- genetic type, and
- infill material.

Figure 2.1 illustrates an example of the influence of a series of steeply dipping faults, which are striking sub parallel to the tunnel axis on the displacements. A stress concentration between fault and left sidewall leads to significantly larger displacements on the left side, while on the right side, the influence of the fault is still minor. (Schubert, 2010).

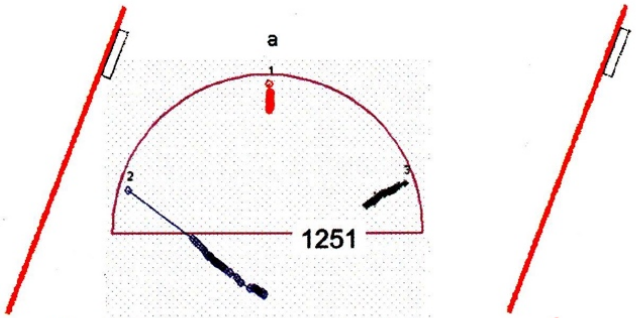

Figure 2.1: Displacement vector plot; influence of faults outside the excavation cross section (Schubert, 2010).

Strong anisotropic displacements, caused by slickensides or faults outside the excavation area have been reported at several projects. Figure 2.2 illustrates the situation at the Innsbruck by-pass tunnel, where slickensides and faults caused overstressing of the rock mass, and thus anisotropic and large displacements (Schubert, 1996). Another example (see Figure 2.3) is the large shear failure of the rock mass in the right wall at the western lot of the Arlberg tunnel, caused due to certain characteristic of a fault zone in combination with the negative effect of water (Schubert, 1996).

According to Warburton (1981), Shi & Goodman, (1985), an extensive unfavourable oriented discontinuity, close-by an excavation boundary can cause rigid block failures containing sliding, falling or toppling mechanism, or a mix of them.

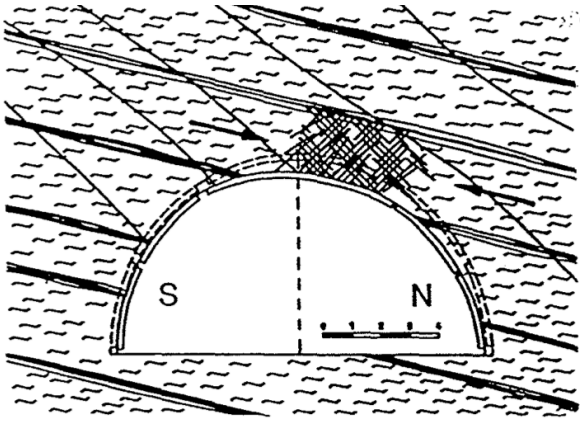

Figure 2.2: Squeezing of a rock into tunnel at Innsbruck by-pass tunnel (Schubert, 1996).

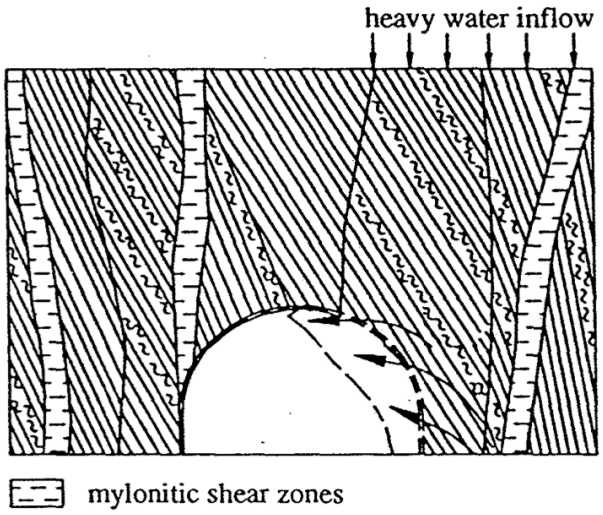

Figure 2.3: Large shear failure at western lot of Arlberg tunnel (Schubert, 1996).

A quotation that highlights the significance of the detection of joints:

"The effect of discontinuities on the stress distribution and failure in the rock mass requires careful studies in each individual case. The early detection of such scenarios before failure must receive the main attention" (Wulf Schubert, 1993).

2.1 Modelling of discontinuities with the finite element method

The most applied numerical method for many advanced rock mechanics simulations of non-linear, anisotropic and time-depended behaviour is the finite element method. It can account for non-linear material behaviour, material heterogeneity, and complex algometric conditions. A big advantage of finite element method is the possibility of representing heterogeneous rocks, with the opportunity to assign various material properties to different finite elements (Nikolić et al., 2016). On the other hand, modelling of discontinuities is limited with the finite element method (Ibrahimbegovic, 2009; Wriggers, 2008).

A first improvement of that problem was the smeared-crack models (de Borst et al., 2004), which allows defining orientations with different shear strength. Another method was an indirect representation of the discontinuities with so called "joint" elements. The constitutive laws of the discontinuities are considering the influence on physical behaviour of the joint elements as equivalent continuum. However, due to the fact, that these joint elements are not able to perform large displacements of discontinuities due to the continuum assumptions, no real detachment is possible with them. The "Goodman joint element", developed especially for rock applications (R. Goodman, 1976; R. Goodman et al., 1968) , was the first element of this kind. Afterwards, improvements of the joint elements were done (Buczkowski & Kleiber, 1997; Desai et al., 1984; Ghaboussi et al., 1973; Zienkiewicz et al., 1970).

3 Computational model

The simulations for this master thesis are done with the software Phase^2 9.0 (Rocscience, 2014). Phase^2 is a 2D finite element program and can be used for a wide range of engineering projects including tunnel and excavation design, slope stability, groundwater seepage, probabilistic analysis, consolidation, and dynamic analysis (Rocscience, 2001). Discrete modelling requires the using of a discontinuum model. Phase^2 is using a continuum model, therefore the denotation discrete modelling is technically speaking not completely correct. However, finite element method software is indirectly representing discontinuities with joint elements. Phase^2 is using a zero thickness joint element in order to maintain numerical stability and allowing realistic assessment of the behaviour of discontinuities (Pande et al., 1990). Therefore, within this master thesis this method will be referred to as "Discrete Modelling".

3.1 Model design

In the following section the model design is described more in detail and a schematic representation of the numerical model is illustrated in Figure 3.3.

3.1.1 Model geometry

In order to avoid critical influences of the model boundary conditions on the numerical results, the model has to be large enough to ensure a primary stress state at the model boundaries at each stage. Hence, a quadratic rock block with a length of 300 metres is used. A tunnel excavation with a diameter of 10 metres is situated at centre of the block.

3.1.2 Displacement boundary conditions

The nodes at the vertical model boundaries are fixed in horizontal direction (x-direction) throughout the analysis, beyond the nodes at the horizontal model boundaries in vertical direction (y-direction). Additionally, the nodes at the corners of the model boundaries are fixed in all directions throughout the analysis.

3.1.3 Joint design, domain and normalization

Phase^2 is representing discontinuities through joint elements, in our case situated in a domain at the right side of the tunnel and divided into several segments (Pande et al., 1990). Figure 3.1 is illustrating a detail of the joint elements and its segmentation in Phase^2 (Rocscience, 2014).The material properties of activated and deactivated joint segments are described in chapter 3.2.3.1 and chapter 3.2.3.2. This joint construction enables investigations into various possibilities regarding the distance and lengths of a singular joint. Furthermore, the distance and the length of the joint are normalized to the tunnel diameter (Figure 3.2).

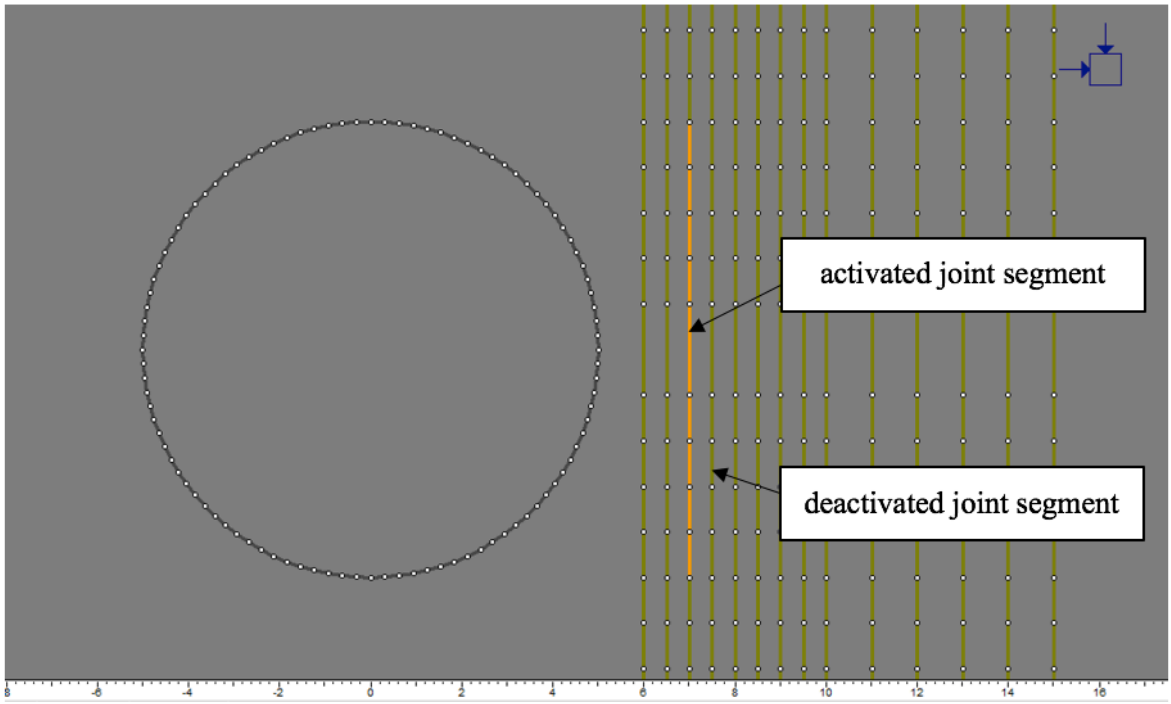

Figure 3.1: Activated and deactivated joint elements and segmentation before meshing in Phase^2.

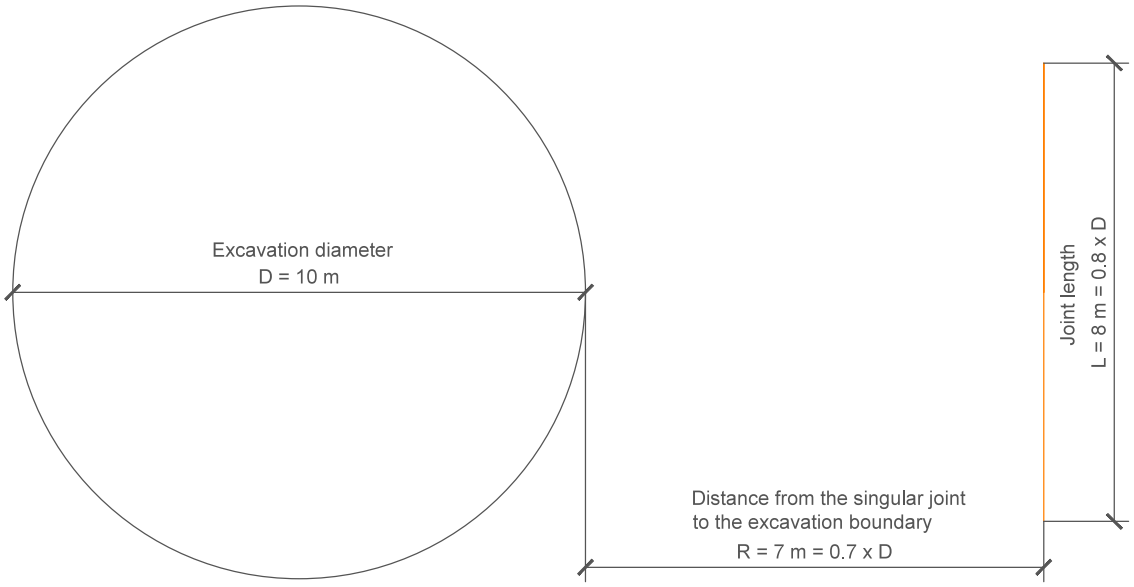

Figure 3.2: Normalization of joint distance R and joint length L to the tunnel diameter D.

3.1.4 Loading

The primary stress state prior to excavation is applied by a constant field stress. For defining a constant field stress, the major in-plane principal field stress σ_1, the minor in-plane principal field stress σ_3, the out-of-plane field stress σ_Z and the angle α_{load} have to be defined. α_{load} is positively measured in counter-clockwise direction, between the positive x-axis and the direction of σ_1.

Two specific cases of the coefficient of the lateral pressure, $K_0 = 0.5$ and $K_0 = 1.0$, are investigated and listed up in Table 3.1 and Table 3.2.

Table 3.1: Constant field stress parameters for $K_0 = 0.5$.

Parameter	Symbol	Value	Unit
Major principal field stress	$\sigma_{1,K=0.5}$	3.90	[MPa]
Minor principal field stress	$\sigma_{3,K=0.5}$	1.95	[MPa]
Out-of-plane field stress	$\sigma_{Z,K=0.5}$	1.95	[MPa]
Angle	$\alpha_{K=0.5}$	90.00	[°]

Table 3.2: Constant field stress parameters for $K_0 = 1.0$.

Parameter	Symbol	Value	Unit
Major principal field stress	$\sigma_{1,K=1.0}$	3.90	[MPa]
Minor principal field stress	$\sigma_{3,K=1.0}$	3.90	[MPa]
Out-of-plane field stress	$\sigma_{Z,K=1.0}$	3.90	[MPa]
Angle	$\alpha_{K=1.0}$	90.00	[°]

3.1.5 Load splitting

The maximal number of iteration steps is set to 2000 with a tolerance of 0.001. To avoid that the simulation is not able to find a numerical equilibrium within these limits, the field stress is applied in six stages. The split factors used are listed up in Table 3.3.

Table 3.3: Load split factors.

Stage	Unit	1	2	3	4	5	6
Split factor	[-]	0.000	0.800	0.900	0.940	0.975	1.000

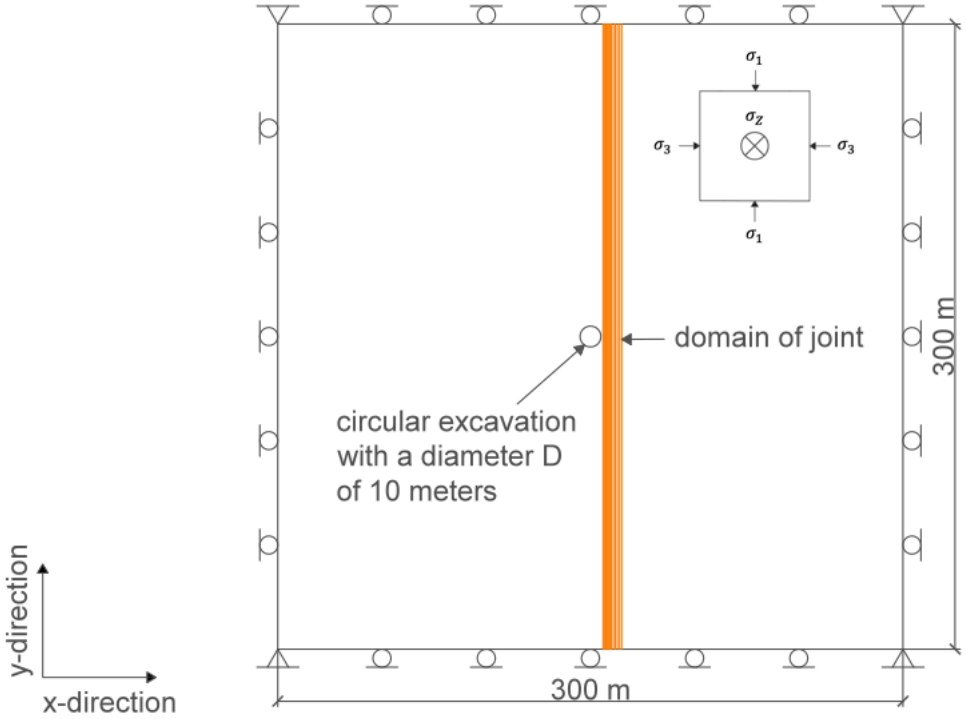

Figure 3.3: Schematic representation of the numerical model.

3.2 Material properties

This chapter is describing failure criterion and the properties of the rock and joint materials. Pore water pressure is not considered for these simulations, therefore the cohesion c and the friction angle φ are total stress parameters.

3.2.1 Material behaviour, failure criterion and material type

For all the simulations, an isotropic, elastic-plastic material behaviour for the rock mass with Mohr Coulomb failure criterion is used.

3.2.2 Rock material properties

For using the Mohr-Coulomb criterion following parameters has to be defined:

- Cohesion of the rock material c_{rock}
- Friction angle of the rock material φ_{rock}
- Tensile strength of the rock material $\sigma_{T,rock}$

Additionally, the dilation angle ψ_{rock} and residual values of cohesion $c_{rock,res}$ friction angle $\varphi_{rock,res}$ and tensile strength $\sigma_{T,rock,res}$ can be defined. The values used for the strength and stiffness for the rock mass are listed up in Table 3.4.

Table 3.4: Rock material properties.

Parameter	Symbol	Value	Unit
Tensile strength peak	$\sigma_{T,rock,peak}$	1.5	[MPa]
Tensile strength residual	$\sigma_{T,rock,res}$	0	[MPa]
Friction angle peak	$\varphi_{rock,peak}$	27	[°]
Friction angle residual	$\varphi_{rock,res}$	23	[°]
Cohesion peak	$c_{rock,peak}$	3.0	[MPa]
Cohesion residual	$c_{rock,res}$	0.5	[MPa]
Dilation angle	ψ_{rock}	0.0	[°]
Young´s Modulus peak	$E_{rock1,peak}$	70000	[MPa]
Young´s Modulus residual	$E_{rock1,res}$	20000	[MPa]
Young´s Modulus peak	$E_{rock2,peak}$	35000	[MPa]
Young´s Modulus residual	$E_{rock2,res}$	10000	[MPa]
Poisson´s Ratio	ν_{rock}	0.25	[-]

3.2.3 Joint material properties

Two different joint material properties are assigned for the simulations. The activated joint segments are simulating the behaviour of the singular joint. All of the other joint segments are assigned with the deactivated joint material properties. These segments should show the same mechanical behaviour as the surrounding rock material.

3.2.3.1 Material properties and slip criterion of activated joint segments

The Mohr-Coulomb slip criterion is used for all activated joint segments. These segments are illustrated as orange coloured joint segments in Phase^2 as illustrated in Figure 3.1 and the used values for the properties are listed up in Table 3.5.

Table 3.5: Material properties of activated joint segments.

Parameter	Symbol	Value	Unit
Tensile strength peak	$\sigma_{T,joint,act,peak}$	0.0	[MPa]
Tensile strength residual	$\sigma_{T,joint,act,res}$	0.0	[MPa]
Friction angle peak	$\varphi_{joint,act,peak}$	0.0	[°]
Friction angle residual	$\varphi_{joint,act,res}$	0.0	[°]
Cohesion peak	$c_{joint,act,peak}$	0.0	[MPa]
Cohesion residual	$c_{joint,act,res}$	0.0	[MPa]
Normal Stiffness	Kn_{act}	35,000	[MPa/m]
Shear Stiffness	Ks_{act}	3,500	[MPa/m]

3.2.3.2 Material properties and slip criterion of deactivated joint segments

A material dependent slip criterion is used for the deactivated joint segments. The joint strength and optional stiffness for the deactivated joint segments are derived from the rock material through the joint segments pass. The interface coefficient Ci considers the material dependent joint strength and is used as a multiplier of the cohesion c_{rock} and the friction angle φ_{rock} of the surrounding rock material. The equations, used for this determination, are as follows:

$$C_{joint,deact,peak} = Ci * C_{rock,peak} \quad \text{(Rocscience, 2001)(3.1)}$$

$$C_{joint,deact,res} = Ci * C_{rock,res} \quad \text{(Rocscience, 2001) (3.2)}$$

$$\varphi_{joint,deact,peak} = arctan * \left[tan\left(\varphi_{rock,peak}\right) * Ci\right] \quad \text{(Rocscience, 2001) (3.3)}$$

$$\varphi_{joint,deact,res} = arctan * \left[tan\left(\varphi_{rock,res}\right) * Ci\right] \quad \text{(Rocscience, 2001) (3.4)}$$

The joint stiffness and strength are defined with respect to the surrounding material properties, by using a multiplying stiffness coefficient Cs. The determination of the normal Kn_{deact} and shear joint stiffness Ks_{deact} based on the Young's Modulus E_{rock} of the surrounding rock material is represented as follows:

$$Ks_{deact,peak} = Cs * E_{rock,peak} \quad \text{(Rocscience, 2001) (3.5)}$$

$$Ks_{deact,res} = Cs * E_{rock,res} \quad \text{(Rocscience, 2001) (3.6)}$$

$$Kn_{deact,peak} = 10 * Ks_{deact,peak} \quad \text{(Rocscience, 2001) (3.7)}$$

$$Kn_{deact,res} = 10 * Ks_{deact,res} \quad \text{(Rocscience, 2001) (3.8)}$$

The deactivated joint segments are olive green coloured in Phase^2 and are illustrated in Figure 3.1. The interface and stiffness coefficients are listed up in Table 3.6.

Table 3.6: Interface and stiffness coefficients of deactivated joint segments.

Parameter	Symbol	Value	Unit
Interface coefficient	Ci	1.0	[-]
Stiffness coefficient	Cs	1.0	[-]

3.3 Model mesh

The software Phase^2 is generating the mesh and its density automatically. To increase accuracy of the results, in the area of interest around the excavation a region with increased mesh density was introduced (see Figure 3.4).

As described in chapter 3.1.3, the joint is divided into several parts. Furthermore, two different joint segment materials are also used (see chapters 3.2.3, 3.2.3.1 and 3.2.3.2). This enables an assignment of the activated and deactivated joint material properties after the meshing, therefore the mesh is equal for all simulations. The meshed model in Phase^2 is illustrated in Figure 3.4.

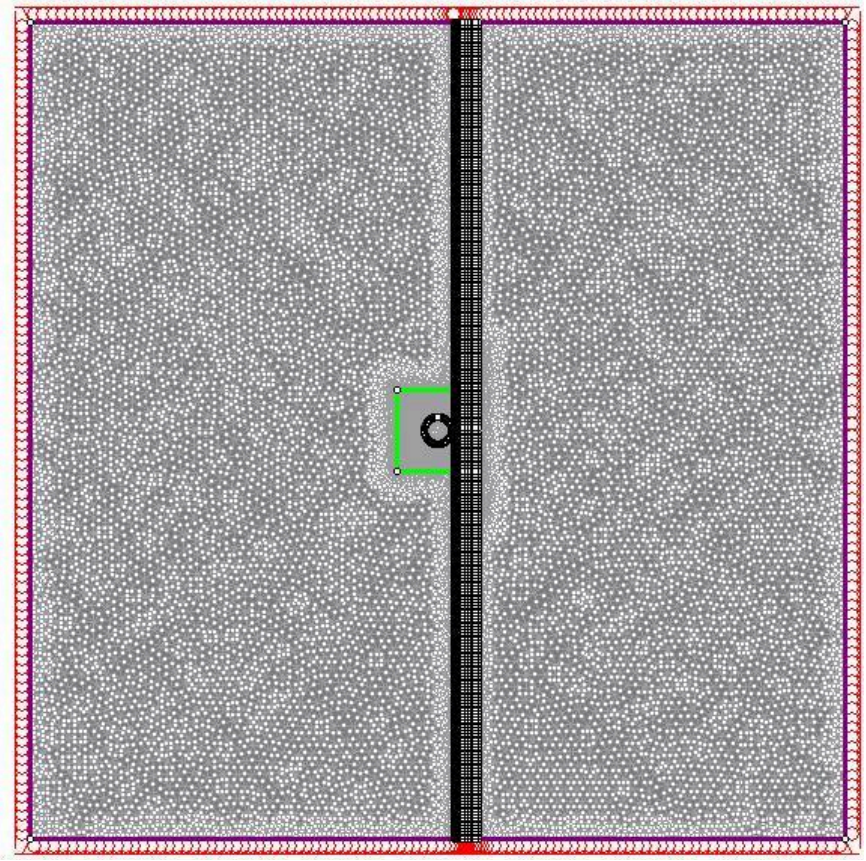

Figure 3.4: Meshed model with boundary conditions before excavation in Phase[2].

3.3.1 Mesh analysis

For investigating the influence of the discretization of the joint segments and the use of material dependent also called “deactivated” joint material, three different models are compared:

- Model I: no joint segments
- Model II: deactivated joint segments on the right side of the excavation area
- Model III: joint segments on the right side of the excavation, but simulated as material boundary segments

The maximum displacement of Model I after the excavation is 0.00035 m, located consistently at the excavation circumference, and illustrated in Figure 3.5. Joint elements with deactivated joint material properties (see chapter 3.2.3.2) are added in Model II. In Modell III, the joint segments are replaced by material boundary segments. This method is used to check if the deactivated joint segments have the same influence on the displacements as the surrounding rock material. Figure 3.6 is demonstrating the results of Model II and Figure 3.7 demonstrates Model III. The maximum displacement of Model II is 0.00042 m and located at the right side wall. For Model III the maximum displacement is also 0.00035 m, like Model I. Thus with comparison of these three models, it can be assumed, that the deactivated joint segments do not show exactly the same behaviour like the surrounding rock material and have a significant effect on the results of the numerical calculations. However, this mesh analysis has shown that the results are highly sensitive to changes in the mesh density.

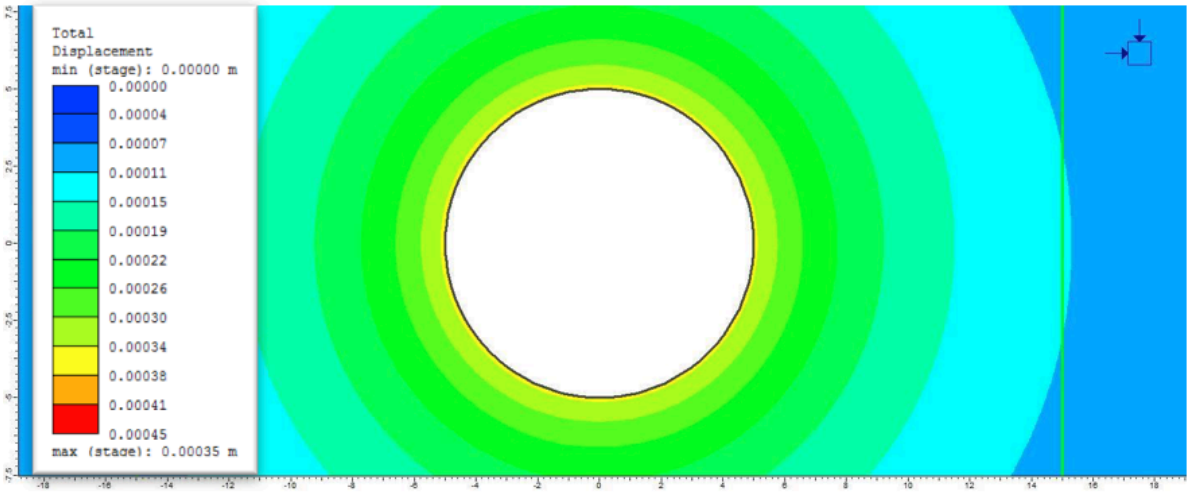

Figure 3.5: Model I, result of the displacements with no deactivated joint segments after excavation in Phase[2].

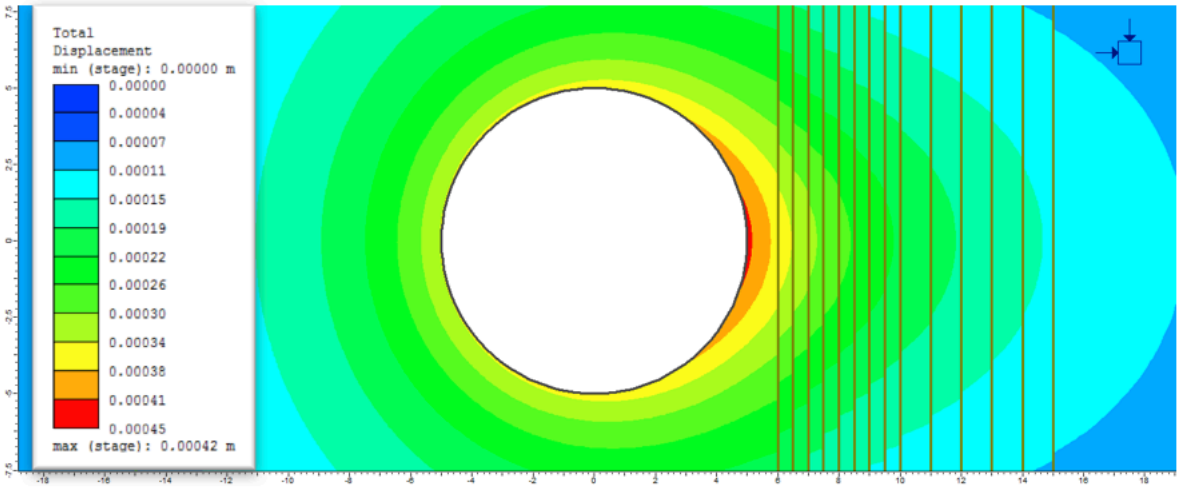

Figure 3.6: Model II, result of the displacements with deactivated joint segments on the right side after excavation in Phase[2].

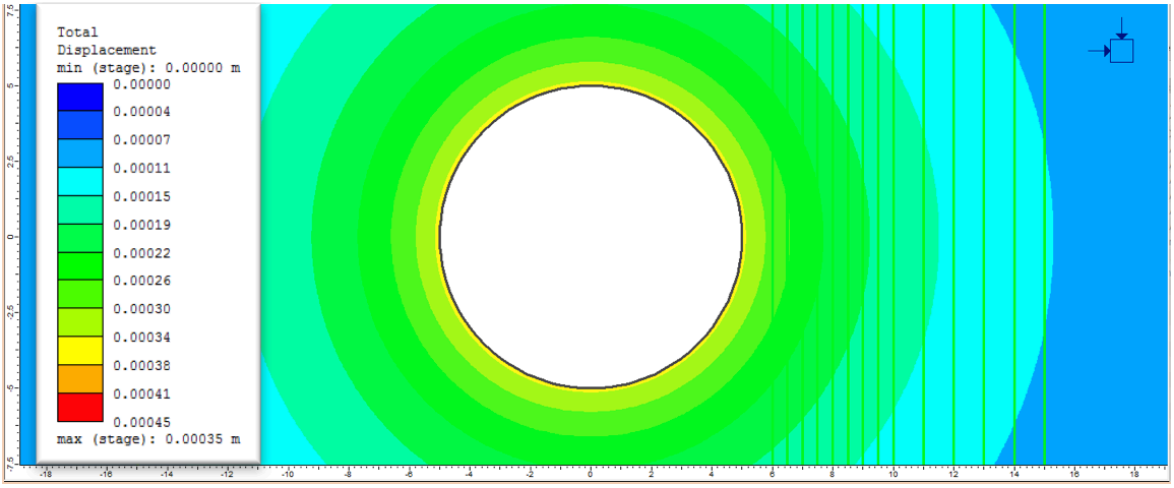

Figure 3.7: Model III, result of the displacements, with deactivated joint segments replaced by material boundary segments on the right side after excavation in Phase[2].

4 Computation

A plane strain analysis is used for all the numerical simulations of the computational models. The solver type is the Gaussian elimination and the metric unit system is used. Table 4.1 lists up the investigated distances from the excavation boundary to the singular joint.

Table 4.1: Investigated distances from excavation boundary to singular joint.

Distance R	Distance from excavation boundary to singular joint	Unit
0.1 D	1	[m]
0.2 D	2	[m]
0.3 D	3	[m]
0.4 D	4	[m]
0.5 D	5	[m]
0.6 D	6	[m]
0.7 D	7	[m]
0.8 D	8	[m]
0.9 D	9	[m]
1.0 D	10	[m]

5 Results

This chapter contains an overview of the numerical results of this thesis. The focus of the investigation is laid on the maximal displacements after excavation. The results of the displacements, for each distance R (see Table 4.1) with various joint lengths, are compared to the associated basic model. When the displacements compared to the reference model increase by more than 50 %, the influence of the joint was considered as significant (see Table 5.1).

Due to the large amount of results, it is not possible to display all the data. Hence, only individual results are illustrated for an exemplarily representation.

5.1 Exemplary results

5.1.1 Reference level of displacements of singular joint for $K_0 = 1.0$.

Figure 5.1 is illustrating the displacements after excavation of the basic model with $K_0 = 1.0$. The maximal displacement of 0.42 mm is multiplied with a factor of 1.5 and used as reference level for the determination of the influence area of a singular joint for $K_0 = 1.0$.

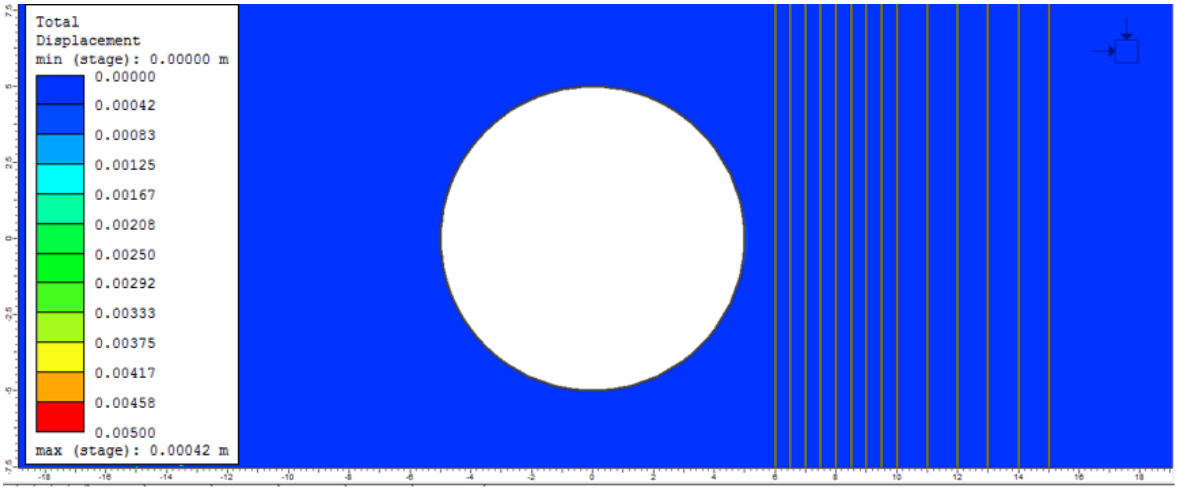

Figure 5.1: Basic model $K_0 = 1.0$, result of the displacements after excavation in Phase[2].

5.1.2 Result of displacements for model $K_0 = 1.0$, R = 0.3 D, L = 3.0 D

The joint distance is 0.3 times the tunnel diameter D and the length is three times D. The displacements after excavation are illustrated in Figure 5.2. The maximum displacement is 2.95 mm and located at the right side wall. Furthermore, the location of a shear or tension failure of the rock material is illustrated in Figure 5.3. The red crosses are figuring a failure in shear and the red circles in tension. In Figure 5.4, the deformation vectors are illustrated with magnification of 500.

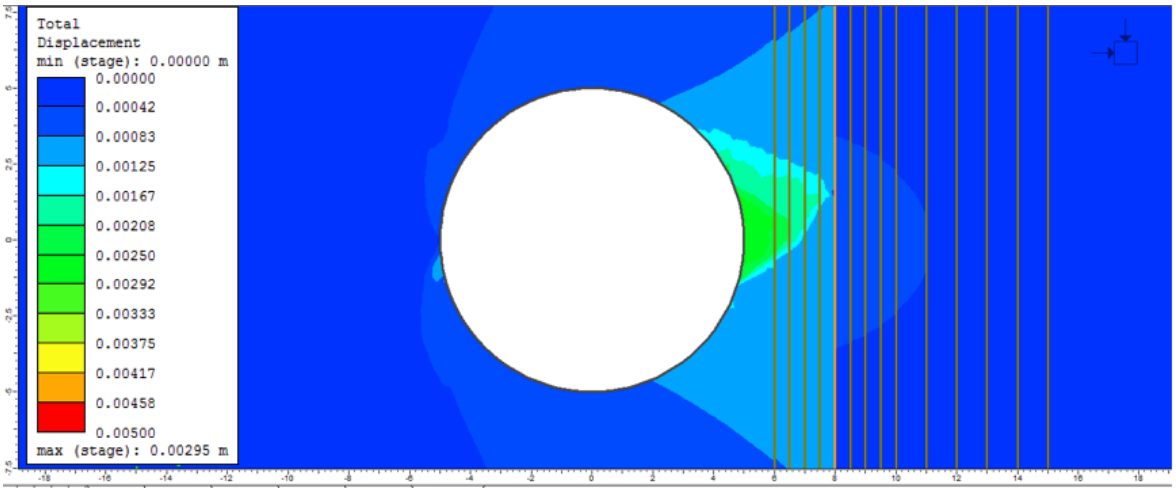

Figure 5.2: Model $K_0 = 1.0$, R = 0.3 D, L = 3.0 D, result of the displacements after the excavation in Phase[2].

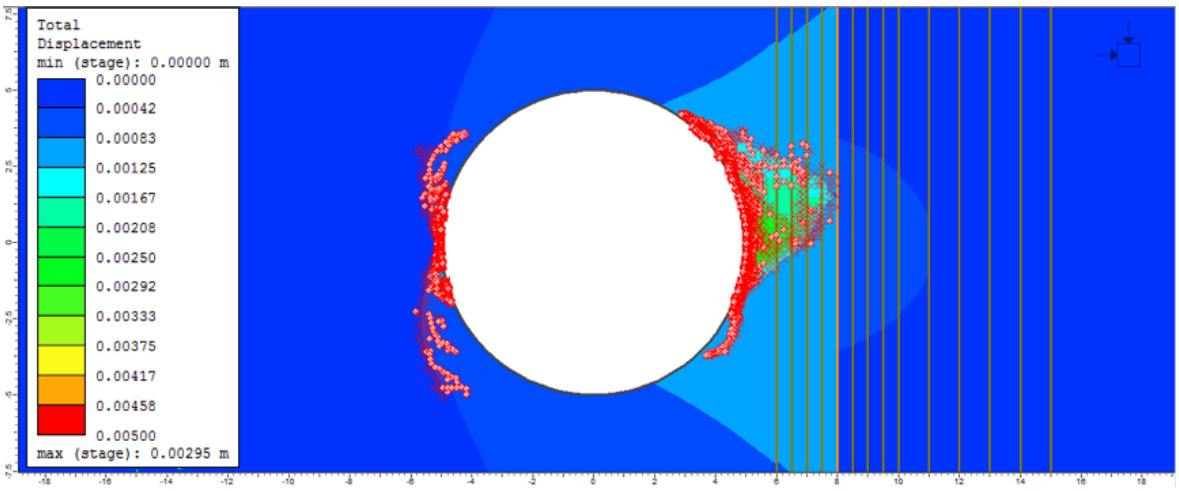

Figure 5.3: Model $K_0 = 1.0$, R = 0.3 D, L = 3.0 D, location of shear and tension failure of the rock material after the excavation in Phase[2].

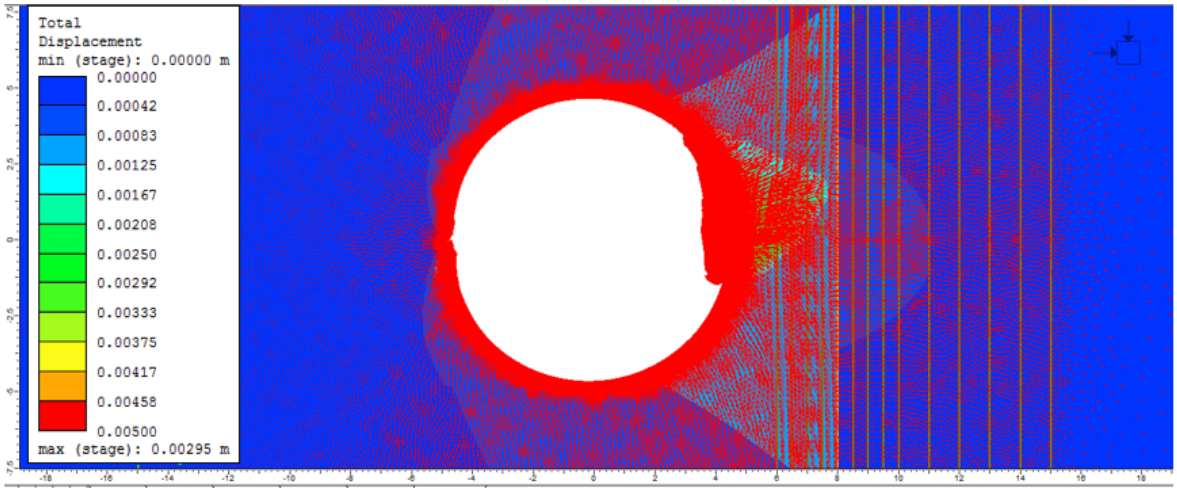

Figure 5.4: Model $K_0 = 1.0$, R = 0.3 D, L = 3.0 D, deformation vectors after the excavation in Phase[2].

5.1.1 Determination of significant influence of a singular joint on displacements

To determine, if a singular joint has a significant influence on the displacement, the displacements are compared to the maximum displacement of the respective basic model. The criteria for the determination of significance are listed up in Table 5.1.

Table 5.1: Determination of significant influence of a singular joint on displacements.

Category	Description	Domain
I	no influence: from zero to normal influence on the displacements	increase from 0 to 50 % of the reference level
II	influence: from normal to high influence on the displacements	increase from 50.1 % or higher

5.1.2 Determination of influence on displacements of various joint lengths with the reference level of the basic model for $K_0 = 0.5$

For this determination, results of models for $K_0 = 0.5$ and R = 0.2 D are shown exemplarily. Figure 5.5 is illustrating the effect of various joint lengths at the same distance R on the displacements. The red line is represents the reference level of the basic model for $K_0 = 0.5$ with a value of 0.8 mm. On the vertical axis the maximal displacements are shown in millimetres, on the horizontal axis the respective joint lengths in relation to the excavation diameter D in m/m.

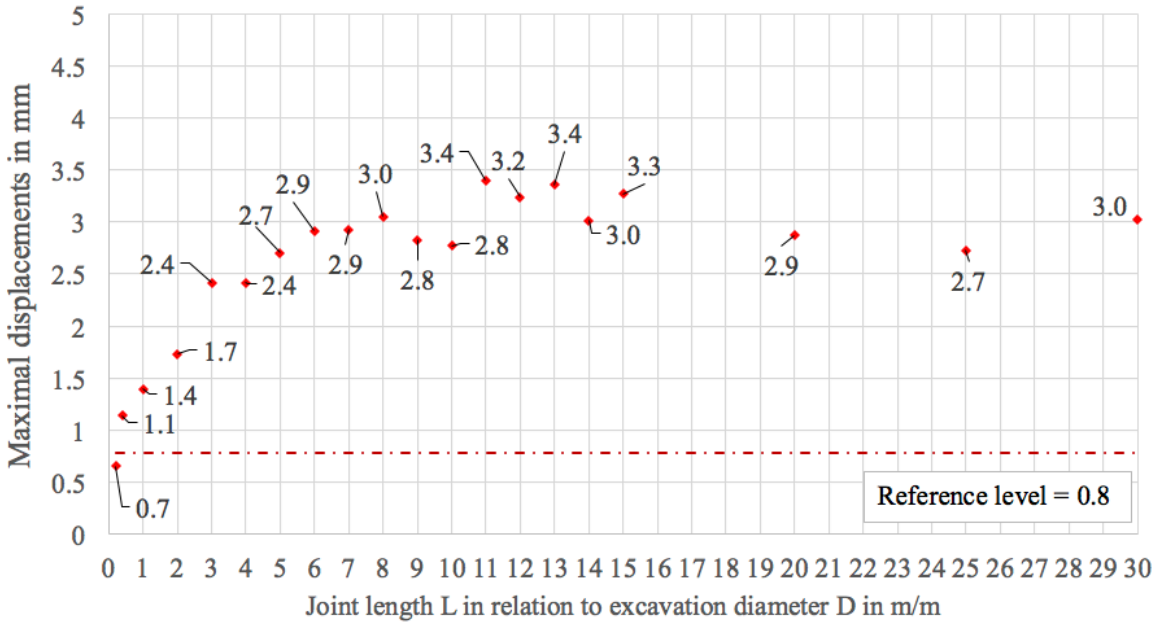

Figure 5.5: Determination of influence of various joint lengths on the displacements for $K_0 = 0.5$, R = 0.2 D.

The results of the displacements of joints with various length and their influence in percentage can be seen in Table 5.2. Furthermore, Table 5.3 shows the classification according to the chosen criterion for significance of influence.

Table 5.2: Displacement results for $K_0 = 0.5$, R = 0.2 D.

Joint length L	Maximal displacement	Unit	Increase of displacement	Unit
0.2 D	0.6	[mm]	25.8	[%]
0.4 D	1.1	[mm]	119.3	[%]
1.0 D	1.4	[mm]	168.0	[%]
2.0 D	1.7	[mm]	233.4	[%]
3.0 D	2.4	[mm]	365.0	[%]
4.0 D	2.4	[mm]	365.4	[%]
5.0 D	2.7	[mm]	419.7	[%]
6.0 D	2.9	[mm]	460.6	[%]
7.0 D	2.9	[mm]	463.9	[%]
8.0 D	3.0	[mm]	486.8	[%]
9.0 D	2.8	[mm]	444.1	[%]
10.0 D	2.8	[mm]	433.0	[%]
11.0 D	3.4	[mm]	554.3	[%]
12.0 D	3.2	[mm]	522.8	[%]
13.0 D	3.4	[mm]	545.7	[%]
14.0 D	3.0	[mm]	480.4	[%]
15.0 D	3.3	[mm]	529.1	[%]
20.0 D	2.9	[mm]	453.0	[%]
25.0 D	2.7	[mm]	425.5	[%]
30.0 D	3.0	[mm]	481.3	[%]

Table 5.3: Categorization of various joint lengths for $K_0 = 0.5$, R = 0.2 D.

Joint length L	Increase of displacement	Unit	Category
0.2 D	25.8	[%]	I
0.4 D	119.3	[%]	II
1.0 D	168.0	[%]	II
2.0 D	233.4	[%]	II
3.0 D	365.0	[%]	II
4.0 D	365.4	[%]	II
5.0 D	419.7	[%]	II
6.0 D	460.6	[%]	II
7.0 D	463.9	[%]	II
8.0 D	486.8	[%]	II
9.0 D	444.1	[%]	II
10.0 D	433.0	[%]	II
11.0 D	554.3	[%]	II
12.0 D	522.8	[%]	II
13.0 D	545.7	[%]	II
14.0 D	480.4	[%]	II
15.0 D	529.1	[%]	II
20.0 D	453.0	[%]	II
25.0 D	425.5	[%]	II
30.0 D	481.3	[%]	II

5.2 Influential areas for singular joint

This chapter shows the influential areas with two different Young's Moduli of the rock mass for $K_0 = 0.5$ and $K_0 = 1.0$. The vertical axis displays what length of the joint related to the diameter D is needed to have a significant influence on the displacements (see Table 5.1). The horizontal axis represents the associated distances in relation to the diameter D.
When the singular joint is within the area below of the line, it has no significant influence on displacements.

5.2.1 Range of influence for $K_0 = 0.5$

Figure 5.6 is illustrating the range of influence for $K_0 = 0.5$ with a Young's Modulus of 70 GPa for the rock mass. The influence of a joint starts at a distance of R = 1.0 D with a length of 20 D and ends at R = 0.1 D with a length of 0.2 D.

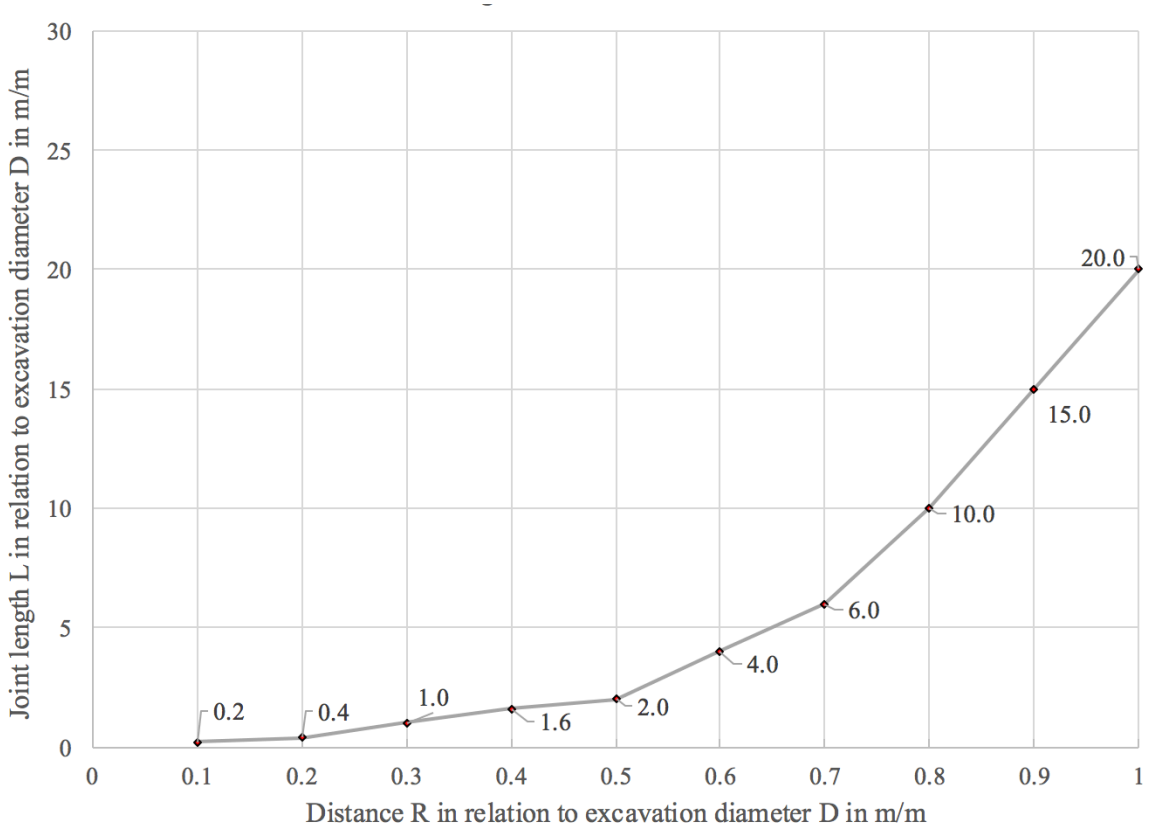

Figure 5.6: Range of influence for $K_0 = 0.5$ of a singular joint.

5.2.1 Range of influence for $K_0 = 1.0$

The range of influence for $K_0 = 1.0$ with a Young's Modulus of 70 GPa for the rock mass is illustrated in Figure 5.7 Before the tunnel reaches a distance R from 0.6 times diameter D to the joint, no significant influence of a singular joint is monitored. At a distance R of 0.6 times diameter D a joint with a length of nine times diameters D is needed to cause a significant influence.

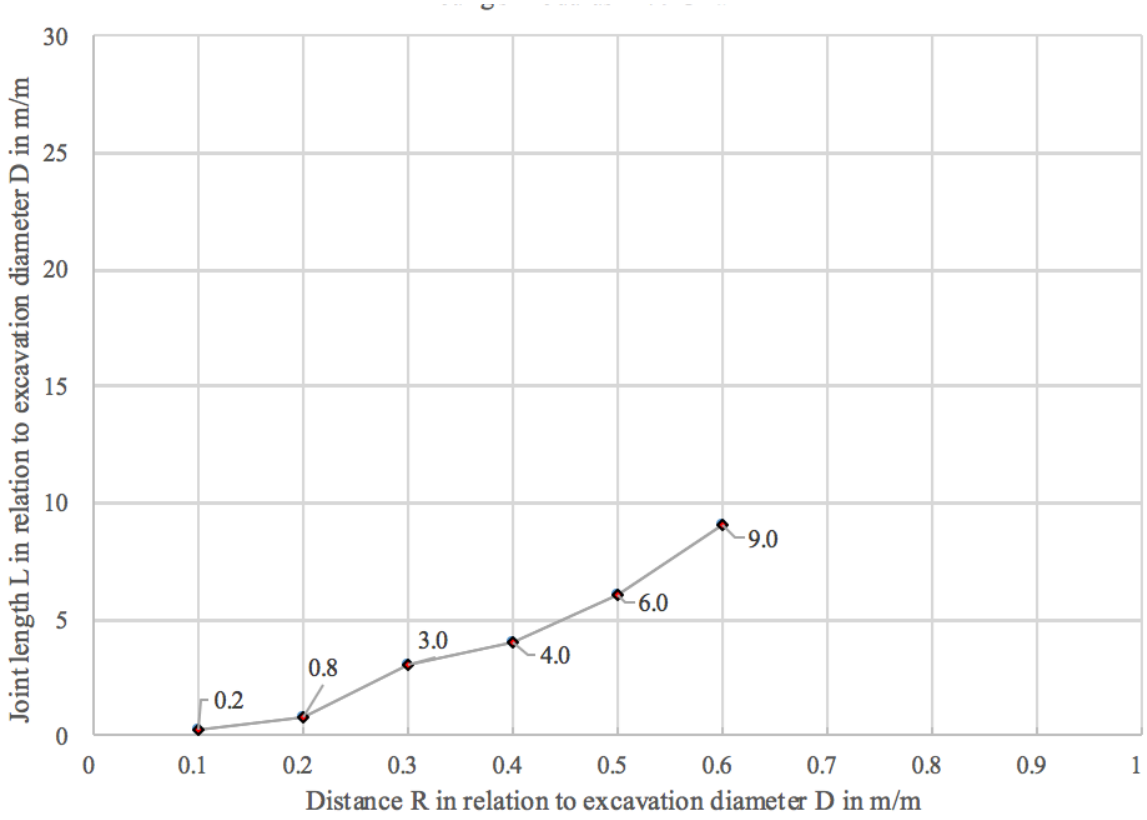

Figure 5.7: Range of influence for $K_0 = 1.0$ of a singular joint.

5.2.1 Range of influence for $K_0 = 1.0$ with decrease of Young's Modulus of rock material

The range of influence for $K_0 = 1.0$ with a Young's Modulus of 35 GPa for the rock mass is illustrated in Figure 5.8. Before the tunnel reaches a distance R from 0.7 times diameter D to the joint, no significant influence of a singular joint is monitored. At a distance R of 0.7 times diameter D a joint with a length of 18 times diameters D is needed to cause a significant influence.

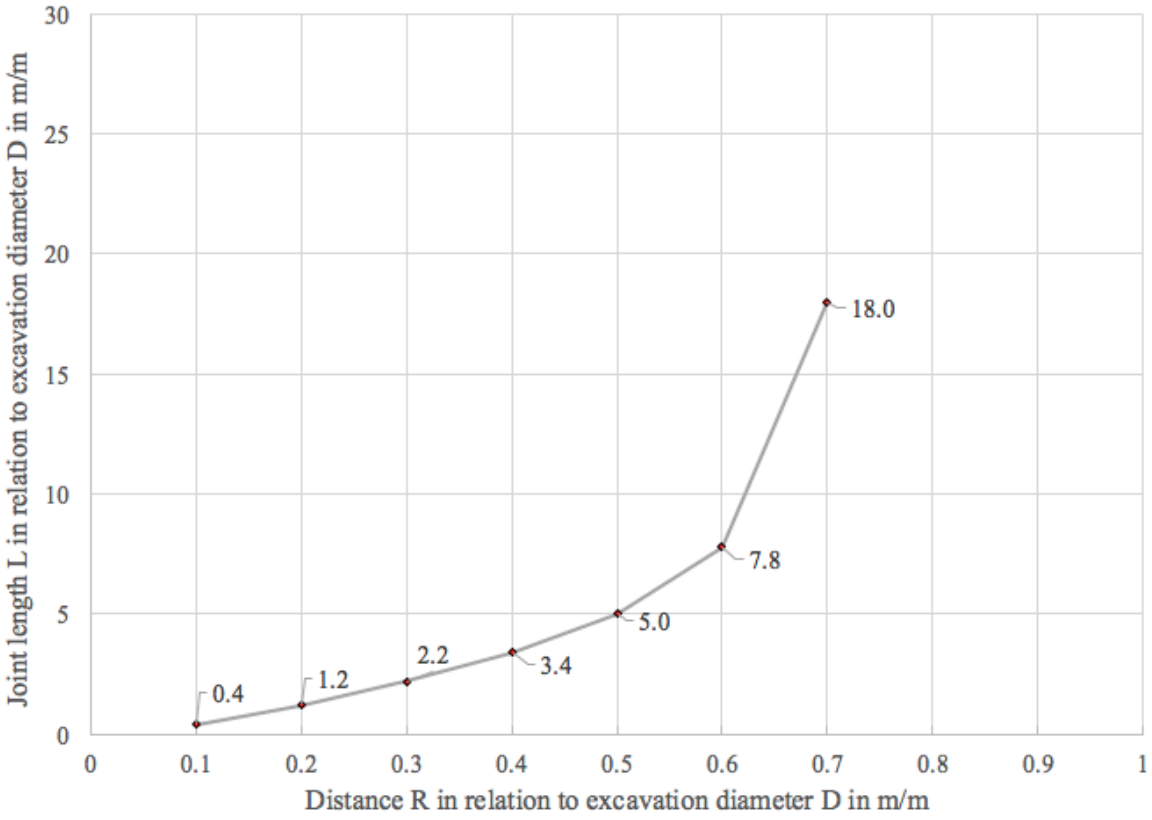

Figure 5.8: Range of influence for $K_0 = 1.0$ of a singular joint.

5.2.1 Comparison of influential areas of different K_0 values

Figure 5.9 shows the comparison of the results for the influential areas for different K_0 values. The green line demonstrates the influence area for $K_0 = 0.5$, the black for $K_0 = 1.0$.

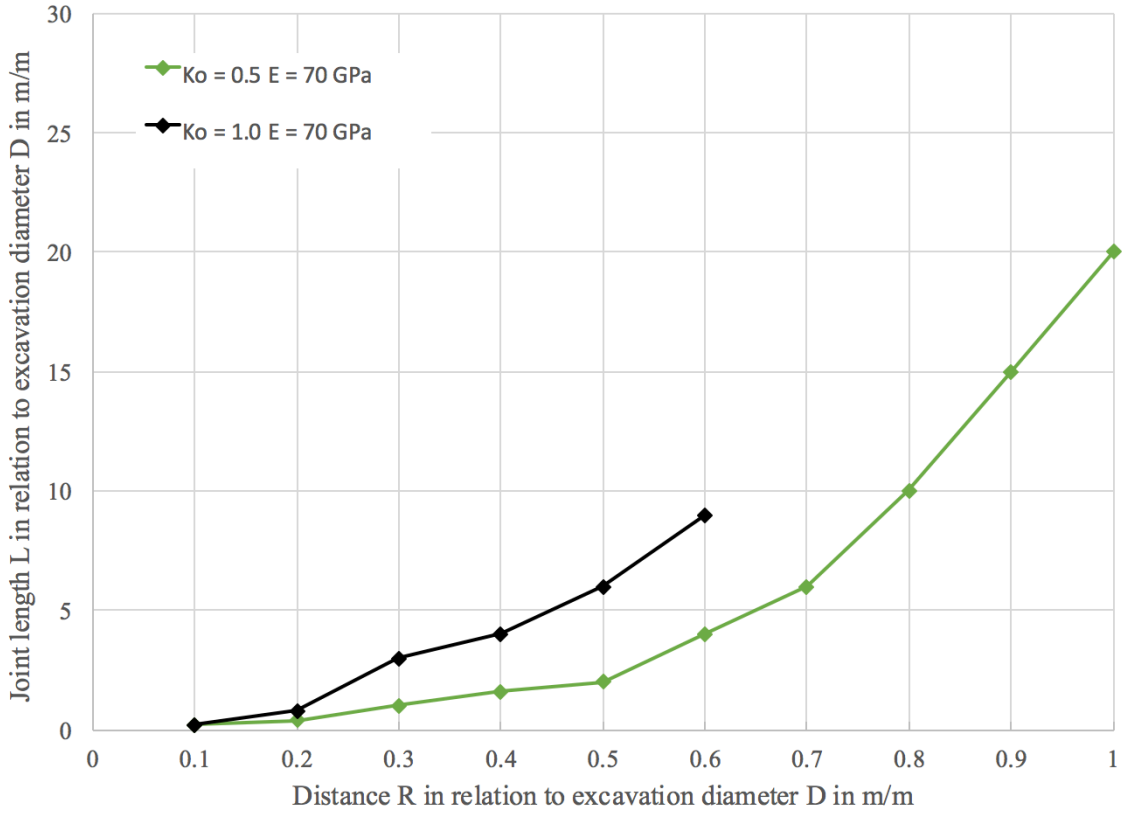

Figure 5.9: Influential areas with same Young's Moduli of rock mass and different K_0 values.

5.2.2 Comparison of influential areas of different Young's Modulus of rock mass

Figure 5.10 shows the comparison of the results for the influential areas for different Young's Modulus of the rock mass. The blue line demonstrates the influence area for $E_{rock2,peak}$ = 35 GPa, the black one for $E_{rock1,peak}$ = 70 GPa.

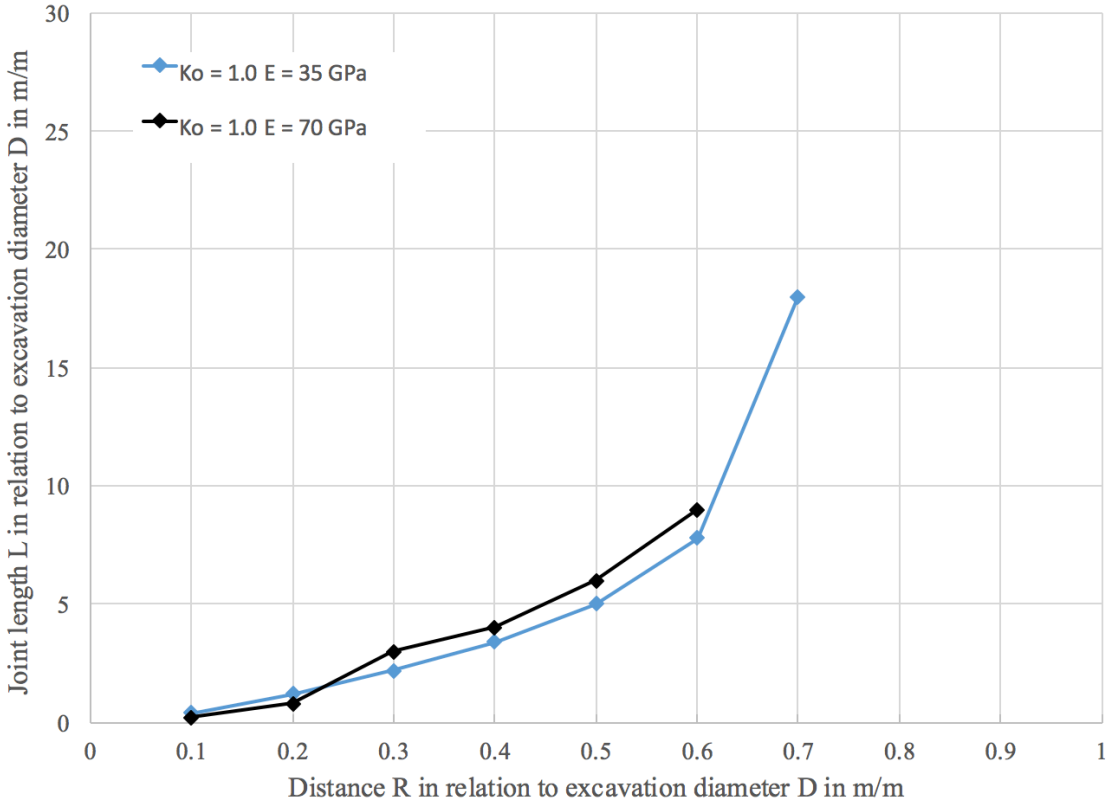

Figure 5.10: Influential areas for $K_0 = 1.0$ with different Young's Moduli of rock mass.

5.3 Visualisation of the influential areas

The results of the investigated influential areas can be seen in Figure 5.11. The lines represent cases, where the influence of the joints was considered significant. An overview of the joint lengths with the corresponding distances, from the excavation cross section to the singular joint, for a significant influence are listed up in Table 5.4.

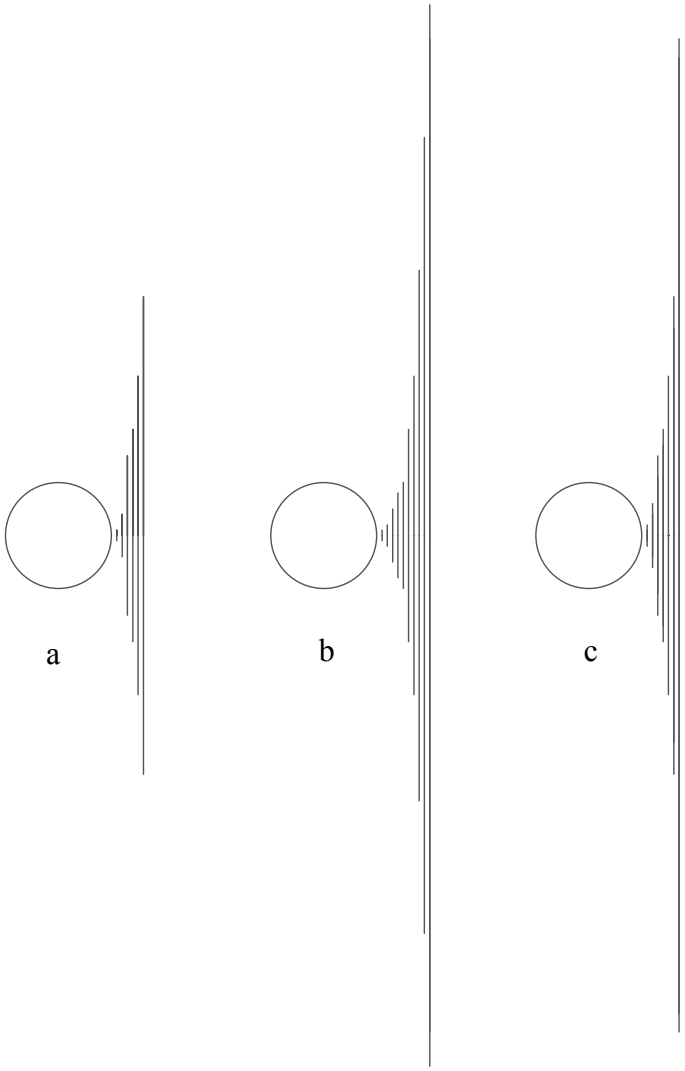

Figure 5.11: Visualisation of results of influential areas on displacements in tunnels; a) influence area for K_0 = 1.0, E_{rock} = 70 GPa; b). influence area for K_0 = 0.5, E_{rock} = 70 GPa; c) influence are for K_0 = 0.5, E_{rock} = 35 GPa.

Table 5.4: Overview of length and distance of the singular joint for a significant influence on displacements.

Distance R	Joint length L a	Joint length L b	Joint length L c
0.1 D	0.2 D	0.2 D	0.4 D
0.2 D	0.8 D	0.4 D	1.2 D
0.3 D	3.0 D	1.0 D	2.2 D
0.4 D	4.0 D	1.6 D	3.4 D
0.5 D	6.0 D	2.0 D	5.0 D
0.6 D	9.0 D	4.0 D	7.8 D
0.7 D	no influence	6.0 D	18.0 D
0.8 D	no influence	10.0 D	no influence
0.9 D	no influence	15.0 D	no influence
1.0 D	no influence	20.0 D	no influence

6 Discussion and Interpretation

This chapter contains a discussion of model design, model mesh and a comparison between the three different models of the numerical simulation. Furthermore, chapter 6.2 is showing the influence of a different K_0 value, chapter 6.3 the influence of a decrease of the Young Modulus of the rock mass.

6.1 Model design and mesh

The mesh analysis in chapter 3.3.1 has shown, that the design of the joint network (see chapter 3.1.3) and the material of the deactivated joint segments (see chapter 3.2.3.2) has an influence on the results of the numerical simulation. Although the joint segments should have the same behaviour like the surrounding rock mass, the simulation is affected.

6.2 Comparison of different K_0 values

As it can be seen in Figure 5.9, the range of influence of a singular joint for $K_0 = 0.5$ starts at R= 1.0 D with a joint length of 20 times diameter D and ends at R = 0.1 D with a length of 0.2 times excavation diameter. For $K_0 = 1.0$ the range of influence starts at a distance of R = 0.6 D with a length of L = 9.0 D and ends at R = 0.1 D with a length of 0.2 D. Therefore, it can be seen, is a tunnel approaching a singular joint in a rock mass with a $K_0 = 0.5$, it can be detected earlier than in a rock mass with $K_0 = 1.0$.

6.3 Comparison of different Young Moduli

As illustrated in Figure 5.10, decrease of the Young's Modulus of the rock mass leads to increase of the influence range of a singular joint. Although the influential areas from the distance R = 0.6 D to R = 0.1 D are nearly similar, the decrease of the Young's Modulus of the rock mass increases the distance R from 0.6 to 0.7 times diameter D.

7 Conclusion

This master thesis has shown, that the range of influence for a singular joint on the displacements in tunnelling is determined by the K_0 value and the Young's modulus of the rock mass. Figure 5.9 has shown, that the K_0 value has a massive effect on the range of influence, when a singular joint can be detected. Furthermore, it can be said that the existence of a lower Young's Modulus of the rock mass leads to an earlier detection when a tunnel is approaching a singular joint (see Figure 5.10).

8 Bibliography

Attewell, P. B., & Woodman, J. P. (1971). Stability of discontinuous rock masses under polyaxial stress systems; Stability of Rock Slopes 13th Symposium on Rock Mechanics, Ed. E. J. Cording, Publ. ASCE, University of Illinois, Urbana, Ill., U.S.A. Aug/Sept 1971, pp.665-683.

Buczkowski, R., & Kleiber, M. (1997). Elasto-plastic interface model for 3D-frictional orthotropic contact problems. *International Journal for Numerical Methods in Engineering*. https://doi.org/10.1002/(SICI)1097-0207(19970228)40:4<599::AID-NME81>3.0.CO;2-H

de Borst, R., Remmers, J. J. C., Needleman, A., & Abellan, M. A. (2004). Discrete vs smeared crack models for concrete fracture: Bridging the gap. *International Journal for Numerical and Analytical Methods in Geomechanics*. https://doi.org/10.1002/nag.374

Desai, C. S., Zaman, M. M., Lightner, J. G., & Siriwardane, H. J. (1984). Thin-layer element for interfaces and joints. *International Journal for Numerical and Analytical Methods in Geomechanics*. https://doi.org/10.1002/nag.1610080103

Fookes, P.G., & Parrish, D. G. (1969). Observations on small-scale structural discontinuities in the London Clay and their relationship to regional geology. *Q. J. Eng. Geol.*, 1, 217 - 240.

Ghaboussi, J., Wilson, E. L., & Isenberg, J. (1973). Finite Element for Rock Joints and Interfaces. *Soil Mechanics and Foundations Division*.

Goodman, R. (1976). Methods of geological engineering in discontinous rock. *West Publishing Company*.

Goodman, R., Taylor, R., & Brekke, T. (1968). A model for the mechanics of jointed rock. *Journal of Soil Mechanics and Foundation Division*.

Ibrahimbegovic, A. (2009). Nonlinear solid mechanics. *Solid Mechanics and Its Applications*. https://doi.org/10.1007/978-90-481-2331-5_1

Nikolić, M., Roje-bonacci, T., & Ibrahimbegović, A. (2016). Overview of the numerical methods for the modelling of rock mechanics problems. *Tehnicki Vjesnik - Technical Gazette*, *23*(2), 627–637. https://doi.org/10.17559/TV-20140521084228

Palmström, A. (2001). Measurement and characterizations of rock mass jointing. *In-Situ Characterizations of Rock*.

Pande, G. N., Beer, G., & Williams, J. R. (1990). *Numerical Methods in Rock Mechanics*. John Wiley & Sons LTD.

Priest, S. D. and Hudson, J. A. (1976) Discontinuity spacings in rock (In Press)

Piteau, D. R., & Jennings, J. E. (1970). The effects of plan geometry on the stability of natural slopes in rock in the Kimberley area of South Africa. In *Proceedings of the 2nd Congress of the International Society of Rock Mechanics (Belgrade)*. https://doi.org/10.1145/2039370.2039408

Rocscience. (2001). *User's Guide Phase2* (Version 7.).

Rocsciene. Phase 2 : 2D finite element stress analysis code. (2014). Rocscience.

Schubert, W. (1996). Dealing with squeezing conditions in alpine tunnels. *Rock Mechanics and Rock Engineering*. https://doi.org/10.1007/BF01032651

Schubert, W. (2010). Lecture notes: Interpretation of displacement monitoring data. Course NATM Engineer, unpublished.

Shi, G. -H, & Goodman, R. E. (1985). Two dimensional discontinuous deformation analysis. *International Journal for Numerical and Analytical Methods in Geomechanics*. https://doi.org/10.1002/nag.1610090604

Warburton, P. M. (1981). Vector stability analysis of an arbitrary polyhedral rock block with any number of free faces. *International Journal of Rock Mechanics and Mining Sciences And*. https://doi.org/10.1016/0148-9062(81)90005-X

Wriggers, P. (2008). *Nonlinear finite element methods*. *Nonlinear Finite Element Methods*. https://doi.org/10.1007/978-3-540-71001-1

Zienkiewicz, O. C., Best, B., Dullage, C., & Stagg, K. G. (1970). Analysis of Nonlinear Problems in Rock Mechanics with Particular Reference to Jointed Rock Systems. In *2nd International Society of Rock Mechanics, Proceedings*.